Effect of Signal-Dependent Shot Noise on Visible Light Positioning

Ahmad Cheema, *Senior Member, IEEE*, Malek Alsmadi, *Member, IEEE*, and Salama Ikki, *Senior Member, IEEE*

***Abstract*—This paper investigates the error bounds for position estimation in downlink visible light communication (VLC) systems. More precisely, we use Cramér-Rao lower bounds (CRLBs) to study the effect of signal-dependent shot noise (SDSN) on the error performance in visible light positioning. We consider synchronous, quasi-synchronous, and asynchronous visible light positioning (VLP) systems. The system performance is assessed based on the position estimation, and uses information from parameters relating to the time of arrival (TOA), time difference of arrival (TDOA), and received signal strength (RSS). The results demonstrate that SDSN has a negative impact on the error bounds in all considered scenarios. Moreover, the level of degradation observed is not uniform among all cases at higher SDSN levels.**

***Index Terms*—Cramér-Rao lower bound, signal-dependent shot noise, visible light positioning.**

I. Introduction

THERE has been great enthusiasm in the literature for visible light communication (VLC)-based positioning and localization techniques. Visible light positioning (VLP) systems have demonstrated better localization accuracy than radio frequency (RF) based positioning, global positioning, and other existing systems. VLP systems have many advantages due to the inherent properties of VLC [1]. Furthermore, VLP systems are used in scenarios where RF communication is subject to multipath fading or RF-inappropriate environments (e.g., underwater and underground), or in spaces where RF radiation is not permitted (e.g., in aeroplanes and hospital magnetic resonance imaging rooms) [1], [2].

The VLP system's performance is traditionally evaluated in the literature by calculating the Cramér-Rao lower bound (CRLB), which is the benchmark for providing theoretical limits on position estimation accuracy. The CRLB offers a lower bound for the variance of any unbiased estimator [3]. The works in [4]–[6] calculated the CRLBs for the distance and 3D position estimations in synchronous VLC systems using time of arrival (TOA) measurements, while [7] carried out a performance analysis for a technique using time difference of arrival (TDOA). In addition, several works investigated asynchronous VLC systems using received signal strength (RSS)-based methods [6], [8]–[14].

Manuscript received March 11, 2022; revised April 20, 2022; accepted April 24, 2022. Date of publication April 27, 2022; date of current version May 5, 2022. *(Corresponding author: Ahmad Cheema.)*

The authors are with the Department of Electrical Engineering, Lakehead University, Thunder Bay, ON P7B 5E1, Canada (e-mail: acheema@lakeheadu.ca; malsamdi@lakeheadu.ca; sikki@lakeheadu.ca).

Digital Object Identifier 10.1109/JPHOT.2022.3170693

Despite their powerful properties, VLP systems face numerous challenges. Firstly, there is signal-dependent shot noise (SDSN), which is noise generated by the LED's transmitted signal at the receiver. Secondly, there is thermal noise, which is caused by the random motion of free electrons in a conductor. This is usually the result of thermal agitation. It is worth mentioning that the largest contributor to thermal noise is the amplifier connected to the photodetector. Next, there is the visible light multipath effect, which is caused by reflection, refraction, and scattering. This can occur upon interaction with a wide range of objects, e.g., glass walls or human clothing, and it can impair the field of view (FOV) or line of sight (LOS). Finally, there is the possibility for errors in synchronization, primarily due to a timing bias between the clocks at the transmitter and receiver. There are other obstacles as well, such as LED tilt position, signal collisions, and mobility issues [1], [2], [15].

The effect of shot noise on VLP accuracy was studied in [4], [8], [10], [11], [14]. These works considered the shot noise as an additive white Gaussian noise (AWGN) with fixed variance, which does not reflect its true nature [16]. Moreover, visible light communication systems with SDSN were studied for capacity bounds, transceiver design, and modulation design [17]–[20]. In this work, we study the effect of ζ_n^2 and our results represent a benchmark that can be considered when the system operates under the joint effects of SDSN and thermal noise. In addition, the CRLB analysis in this paper is valid for any value of ζ_n^2. The results indicate that SDSN significantly impacts the CRLBs for all studied cases. However, it is not necessary for each estimator to reach this bound. That said, the designer should be able to consult a benchmark performance in the event that SDSN does impact the system. Here, we consider synchronous, quasi-synchronous, and asynchronous scenarios. Performance assessment is based on position estimations employing information from TOA, TDOA, RSS, and hybrid parameters.

To the best of the authors' knowledge, the literature has yet to consider the time dependency of SDSN when calculating the error bounds for 3D positioning in VLC systems. Based on this, and motivated by the importance and timeliness of this topic, this paper investigates the error bounds for 3D position estimation in downlink VLC systems. More precisely, we study the joint effects of SDSN and thermal noise on the estimation error bounds. When evaluating the positioning error's CRLBs, we consider synchronous, quasi-synchronous, and asynchronous VLC systems. Performance assessment is done through the use of hybrid TOA-RSS, hybrid TDOA-RSS, and RSS parameters.

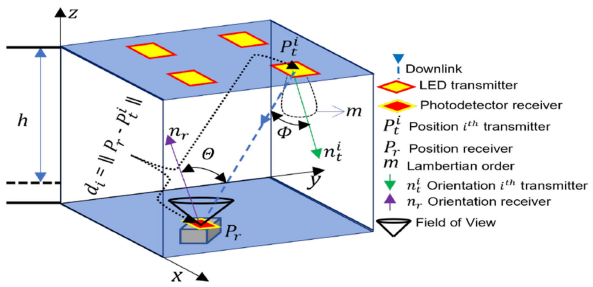

Fig. 1. VLP system model schematic diagram.

Furthermore, in the simulation and performance analysis section, we studied the ratio between the variances of SDSN and thermal noise, which is represented by ζ_n^2. Our results represent a benchmark that can be considered when the system is under the joint effects of SDSN and thermal noise. In addition, the CRLB analysis in this paper is valid for any value of ζ_n^2. The results indicate that SDSN significantly impacts the CRLBs for all studied cases. However, not all the estimators need to reach this bound, but the designer should be able to consult a benchmark in the event that the system is affected by SDSN.

The rest of the paper is organized as follows: Section II describes the setup of the VLP system under the effects of SDSN and thermal noise. Section III evaluates the CRLB for synchronous, quasi-synchronous, and asynchronous scenarios. Simulation and performance analysis are presented in Section IV to supplement the theoretical results. Finally, Section V provides concluding remarks.

II. System Description

This study considers a downlink VLC system with intensity modulation direct detection (IM/DD). There are LEDs at the transmitter and a photodetector at the receiver side, as shown in Fig. 1. Our system is based on a LOS VLC system with no multipath transmission, where the photodetecting receiver lies in the FOV of the light signal emitted by the LED transmitters, keeping in line with the VLP system models in the literature.

In order to avoid signal collision between the LED transmitters, the VLC system utilizes a multiple access protocol (e.g., time-division multiple access (TDMA) and frequency-division multiple access (FDMA)) [15]. Furthermore, the ith LED transmitted signal is received at the photodetecting receiver, which converts the optical signal to an electrical one. The output signal at the receiver side is a delayed and attenuated version of the transmitted pilot signal; it is corrupted by the thermal noise and SDSN, which can be expressed as in [16]

$$r_i(t) = \alpha_i R\, x_i(t-\tau_i) + \sqrt{\alpha_i R\, x_i(t-\tau_i)}\,\xi_{\mathrm{sh}_i}(t) + \xi_{\mathrm{th}_i}(t), \tag{1}$$

where $i \in \{1, \ldots, L_{\mathrm{T}}\}$ and L_{T} is the number of LED transmitters. The optical channel attenuation factor is represented by α_i, and has a real positive value ($\alpha_i > 0$). R denotes the photodetector's responsivity, which is assumed to be constant over the optical bandwidth of the transmitted pilot signal. $x_i(t)$ is the transmitted pilot signal used in the position estimation for $t \in [T_{1,i}, T_{2,i}]$. Here, the observation interval is determined by $T_{1,i}$ and $T_{2,i}$, which completely contains the signal emitted by the ith LED transmitter. The TOA of the transmitted pilot signal by the ith LED at the photodetector receiver is represented by τ_i. $\sqrt{\alpha_i R\, x_i(t-\tau_i)}\,\xi_{\mathrm{sh}_i}(t)$ is the SDSN term and $\xi_{\mathrm{th}_i}(t)$ is the signal-independent thermal noise. Both noises can be modeled as AWGN, where the SDSN variance is dependent on the input signal [16]. Due to the statistics of the additive noise, the elements $(\xi_{\mathrm{sh}_1}(t), \ldots, \xi_{\mathrm{sh}_{L_{\mathrm{T}}}}(t))$ and $(\xi_{\mathrm{th}_1}(t), \ldots, \xi_{\mathrm{th}_{L_{\mathrm{T}}}}(t))$ are modeled as independent and identically distributed (i.i.d.) random variables (RV), implying that SDSN $\xi_{\mathrm{sh}_i}(t) \sim N(0, \zeta_n^2\sigma_n^2)$,[1] where the term $\zeta_n^2 > 0$ describes the ratio between the variances of SDSN and thermal noise $\xi_{\mathrm{th}_i}(t) \sim N(0, \sigma_n^2)$ [16].

The downlink optical wireless channel attenuation factor α_i in (1) can be modeled as in [21]

$$\begin{aligned}\alpha_i &= \frac{(m_i+1)A_{\mathrm{p}}}{2\pi d_i^2}\cos^{m_i}(\phi_i)\cos(\theta_i),\\ \alpha_i &= -\frac{(m_i+1)A_{\mathrm{p}}}{2\pi d_i^2}\frac{\left[(\boldsymbol{P}_{\mathrm{r}}-\boldsymbol{P}_{\mathrm{t}}^i)^T\boldsymbol{n}_{\mathrm{t}}^i\right]^{m_i}}{\|\boldsymbol{P}_{\mathrm{r}}-\boldsymbol{P}_{\mathrm{t}}^i\|^{m_i}}\frac{(\boldsymbol{P}_{\mathrm{r}}-\boldsymbol{P}_{\mathrm{t}}^i)^T\boldsymbol{n}_{\mathrm{r}}}{\|\boldsymbol{P}_{\mathrm{r}}-\boldsymbol{P}_{\mathrm{t}}^i\|},\end{aligned} \tag{2}$$

where m_i is the ith LED's Lambertian order, which depends on the approximate Lambertian model $m_i = -(\ln 2/\ln(\cos\phi_{i\frac{1}{2}}))$ with an emission semiangle at half-power $\phi_{i\frac{1}{2}}$. The photodetector's effective area is represented by A_{p}. The Euclidean distance between the photodetecting receiver and the ith LED transmitter is represented by $d_i = \|\boldsymbol{P}_{\mathrm{r}} - \boldsymbol{P}_{\mathrm{t}}^i\|$, where the positions of the receiver and the ith LED transmitter are represented by $\boldsymbol{P}_{\mathrm{r}} = [P_{\mathrm{r,x}}\ P_{\mathrm{r,y}}\ P_{\mathrm{r,z}}]^T$ and $\boldsymbol{P}_{\mathrm{t}}^i = [P_{\mathrm{t,x}}^i\ P_{\mathrm{t,y}}^i\ P_{\mathrm{t,z}}^i]^T$, respectively. ϕ_i and θ_i are arbitrary orientation angles with respective orientation vectors $\boldsymbol{n}_{\mathrm{t}}^i = [n_{\mathrm{t,x}}^i\ n_{\mathrm{t,y}}^i\ n_{\mathrm{t,z}}^i]^T$ and $\boldsymbol{n}_{\mathrm{r}} = [n_{\mathrm{r,x}}\ n_{\mathrm{r,y}}\ n_{\mathrm{r,z}}]^T$ for the ith LED transmitter and the photodetecting receiver.

In (1), the TOA parameter is modeled as

$$\tau_i = \frac{\|\boldsymbol{P}_{\mathrm{r}} - \boldsymbol{P}_{\mathrm{t}}^i\|}{c} + \Delta_i, \tag{3}$$

where c is the speed of light and the photodetecting receiver has a timing bias Δ_i with respect to the ith LED transmitter's clock. The received signal $r_i(t)$ in (1) can be hence re-written as

$$y_i(t) = \alpha_i R\, x_i(t-\tau_i) + \Omega_i(t). \tag{4}$$

Here, $\Omega_i(t) \sim N(0, \Gamma_i)$, where $\Gamma_i = \sigma_n^2(1 + \alpha_i\, R\, x_i(t-\tau_i)\zeta_n^2)$. The system model assumes that A_{P}, R, n_{r}, m_i, P_{t}^i, n_{t}^i, and $x_i(t)$ are known at the photodetecting receiver for all $i \in \{1, \ldots, L_{\mathrm{T}}\}$.

III. Cramér-Rao Lower Bounds

In this section, we study the 3D positioning error bounds in a VLC system under the effects of SDSN. We calculate the CRLBs for synchronous, quasi-synchronous, and asynchronous scenarios depending on information relating to τ_i, and α_i. The probability density function (PDF) of the received signal model

[1] $N(\mu, \sigma_n^2)$ represents the Gaussian distributed RV with μ mean and σ_n^2 variance.

in (4) can be written as

$$\mathrm{f}(Y(t))|P_{\mathrm{r}})=\frac{1}{\sqrt{2\pi\Gamma_i}}\exp\left(-\frac{1}{2\Gamma_i}\left(Y(t)-\alpha_i R\, x_i(t-\tau_i)\right)^2\right). \tag{5}$$

The joint PDF for the received signal vector $\boldsymbol{Y}(t) \triangleq [y_1(t)\cdots y_{L_{\mathrm{T}}}(t)]^T$ can be written as

$$\begin{aligned}&\mathrm{f}(y_i(t))|P_{\mathrm{r}})\\ &=\left(\prod_{i=1}^{L_{\mathrm{T}}}\frac{1}{\sqrt{2\pi\Gamma_i}}\right)\exp\left(-\frac{1}{2}\sum_{i=1}^{L_{\mathrm{T}}}\frac{(y_i(t)-\alpha_i R\, x_i(t-\tau_i))^2}{\Gamma_i}\right).\end{aligned} \tag{6}$$

Now, by observing the interval of the ith transmitted signal, the log-likelihood of (6) can be given as

$$\begin{aligned}\mathcal{L}(\boldsymbol{\varrho}) =& -\frac{L_{\mathrm{T}}}{2}\ln(2\pi)\\ &-\frac{1}{2}\sum_{i=1}^{L_{\mathrm{T}}}\int_{T_{1,i}}^{T_{2,i}}\ln\sigma_n^2\left(1+\alpha_i R x_i(t-\tau_i)\zeta_n^2\right)dt\\ &-\frac{1}{2}\sum_{i=1}^{L_{\mathrm{T}}}\int_{T_{1,i}}^{T_{2,i}}\frac{(y_i(t)-\alpha_i R x_i(t-\tau_i))^2}{\sigma_n^2(1+\alpha_i R x_i(t-\tau_i)\zeta_n^2)}dt,\end{aligned} \tag{7}$$

where $\boldsymbol{\varrho}$ represents the set of unknown parameters that needs to be estimated, including P_r and other nuisance parameters. These depend on the considered scenarios, as investigated in the upcoming pages.

The Fisher information matrix (FIM) of $\boldsymbol{\varrho}$ can be obtained from $\mathcal{L}(\boldsymbol{\varrho})$ as in [3]

$$\boldsymbol{\mathcal{I}}(\boldsymbol{\varrho})=\mathbb{E}\left\{\left(\nabla_{\boldsymbol{\varrho}}\mathcal{L}(\boldsymbol{\varrho})\right)\left(\nabla_{\boldsymbol{\varrho}}\mathcal{L}(\boldsymbol{\varrho})\right)^T\right\}, \tag{8}$$

where $\nabla_{\boldsymbol{\varrho}}$ is the gradient operator. The CRLB is obtained by taking the inverse of the FIM in (8). The estimation error covariance can consequently be expressed as

$$\mathbb{E}\left\{(\hat{\boldsymbol{\varrho}}-\boldsymbol{\varrho})(\hat{\boldsymbol{\varrho}}-\boldsymbol{\varrho})^{\mathrm{T}}\right\}\succeq\boldsymbol{\mathcal{I}}(\boldsymbol{\varrho})^{-1}. \tag{9}$$

$\boldsymbol{A}\succeq\boldsymbol{B}$ means that $\boldsymbol{A}-\boldsymbol{B}\geq 0$, where the relevant interpretation of ≥ 0 is that the matrix is positive and semidefinite [3]. Now, we discuss the CRLBs for three different scenarios depending on the available τ_i and α_i information. We have done this for synchronous, quasi-synchronous and asynchronous estimations.

A. 3D Positioning Estimation in Synchronous System

This scenario studies a perfectly synchronous (i.e., in (3) the timing bias $\Delta_i=0$) VLP system. In this case, the TOA τ_i and the channel attenuation factor α_i parameters information are available. As a result, τ_i and α_i are functions of $\boldsymbol{P}_{\mathrm{r}}$. This scenario is termed hybrid TOA-RSS because information from both τ_i and α_i is used for 3D position estimation. It is also worth mentioning that α_i is related to RSS. Now, based on (2), (3), and (4), the vector containing the set of unknown parameters in (7) becomes $\boldsymbol{\varrho}=[P_{r,x}\ P_{r,y}\ P_{r,z}]^T=\boldsymbol{P}_{\mathrm{r}}$. Now, the FIM $\mathcal{I}_{\mathrm{sync}}$ can be derived from (7) and (8) as

$$\begin{aligned}&[\mathcal{I}_{\mathrm{sync}}]_{v_1,v_2}\\ &=\frac{R^2}{\sigma_n^2}\Bigg(\zeta_n^4\sigma_n^2\sum_{i=1}^{L_{\mathrm{T}}}\Bigg(\frac{\partial\alpha_i}{\partial P_{\mathrm{r},v_1}}\frac{\partial\alpha_i}{\partial P_{\mathrm{r},v_2}}E^i_{BB}+\alpha_i^2\frac{\partial\tau_i}{\partial P_{\mathrm{r},v_1}}\frac{\partial\tau_i}{\partial P_{\mathrm{r},v_2}}E^i_{AA}\\ &\quad-\alpha_i\left(\frac{\partial\alpha_i}{\partial P_{\mathrm{r},v_1}}\frac{\partial\tau_i}{\partial P_{\mathrm{r},v_2}}+\frac{\partial\tau_i}{\partial P_{\mathrm{r},v_1}}\frac{\partial\alpha_i}{\partial P_{\mathrm{r},v_2}}\right)E^i_{CC}\Bigg)\\ &\quad+\sum_{i=1}^{L_{\mathrm{T}}}\Bigg(\frac{\partial\alpha_i}{\partial P_{\mathrm{r},v_1}}\frac{\partial\alpha_i}{\partial P_{\mathrm{r},v_2}}E^i_{B}+\alpha_i^2\frac{\partial\tau_i}{\partial P_{\mathrm{r},v_1}}\frac{\partial\tau_i}{\partial P_{\mathrm{r},v_2}}E^i_{A}\\ &\quad-\alpha_i\left(\frac{\partial\alpha_i}{\partial P_{\mathrm{r},v_1}}\frac{\partial\tau_i}{\partial P_{\mathrm{r},v_2}}+\frac{\partial\tau_i}{\partial P_{\mathrm{r},v_1}}\frac{\partial\alpha_i}{\partial P_{\mathrm{r},v_2}}\right)E^i_{C}\Bigg)\Bigg),\end{aligned} \tag{10}$$

where $v_1, v_2\in\{x,y,z\}$ and

$$\frac{\partial x_i(t-\tau_i)}{\partial P_{\mathrm{r},v_{(1|2)}}}=x_i'(t-\tau_i)\left(-\frac{\partial\tau_i}{\partial P_{\mathrm{r},v_{(1|2)}}}\right), \tag{11}$$

$$\frac{\partial\tau_i}{\partial P_{\mathrm{r},v_{(1|2)}}}=\frac{P_{\mathrm{r},v_{(1|2)}}-P^i_{\mathrm{t},v_{(1|2)}}}{c\|\boldsymbol{P}_{\mathrm{r}}-\boldsymbol{P}^i_{\mathrm{t}}\|}, \tag{12}$$

$$\begin{aligned}\frac{\partial\alpha_i}{\partial P_{\mathrm{r},v_{(1|2)}}}=&-\frac{(m_i+1)A_p}{2\pi}\Bigg(\frac{\left[(\boldsymbol{P}_{\mathrm{r}}-\boldsymbol{P}^i_{\mathrm{t}})^T\boldsymbol{n}^i_{\mathrm{t}}\right]^{m_i-1}}{\|\boldsymbol{P}_{\mathrm{r}}-\boldsymbol{P}^i_{\mathrm{t}}\|^{m_i+3}}\\ &\times\left(m_i\, n^i_{\mathrm{t},v_{(1|2)}}(\boldsymbol{P}_{\mathrm{r}}-\boldsymbol{P}^i_{\mathrm{t}})^T\boldsymbol{n}_{\mathrm{r}}+n_{\mathrm{r},v_{(1|2)}}(\boldsymbol{P}_{\mathrm{r}}-\boldsymbol{P}^i_{\mathrm{t}})^T\boldsymbol{n}^i_{\mathrm{t}}\right)\\ &-\frac{(m_i+3)(P_{\mathrm{r},v_{(1|2)}}-P^i_{\mathrm{t},v_{(1|2)}})}{\|\boldsymbol{P}_{\mathrm{r}}-\boldsymbol{P}^i_{\mathrm{t}}\|^{m_i+5}}\left((\boldsymbol{P}_{\mathrm{r}}-\boldsymbol{P}^i_{\mathrm{t}})^T\boldsymbol{n}^i_{\mathrm{t}}\right)^{m_i}\\ &(\boldsymbol{P}_{\mathrm{r}}-\boldsymbol{P}^i_{\mathrm{t}})^T\boldsymbol{n}_{\mathrm{r}}\Bigg),\end{aligned} \tag{13}$$

with the following signal energies

$$E^i_{\mathrm{A}}\triangleq\int_0^{T_{0,i}}\frac{(x_i'(t))^2}{(1+\alpha_i R\, x_i(t)\zeta_n^2)}dt, \tag{14a}$$

$$E^i_{\mathrm{AA}}\triangleq\int_0^{T_{0,i}}\frac{(x_i'(t))^2}{(1+\alpha_i R\, x_i(t)\zeta_n^2)^2}dt, \tag{14b}$$

$$E^i_{\mathrm{B}}\triangleq\int_0^{T_{0,i}}\frac{(x_i(t))^2}{(1+\alpha_i R\, x_i(t)\zeta_n^2)}dt, \tag{14c}$$

$$E^i_{\mathrm{BB}}\triangleq\int_0^{T_{0,i}}\frac{(x_i(t))^2}{(1+\alpha_i R\, x_i(t)\zeta_n^2)^2}dt, \tag{14d}$$

$$E^i_{\mathrm{C}}\triangleq\int_0^{T_{0,i}}\frac{x_i(t)\,x_i'(t)}{(1+\alpha_i R\, x_i(t)\zeta_n^2)}dt, \tag{14e}$$

$$E^i_{\mathrm{CC}}\triangleq\int_0^{T_{0,i}}\frac{x_i(t)\,x_i'(t)}{(1+\alpha_i R\, x_i(t)\zeta_n^2)^2}dt. \tag{14f}$$

Here, it is assumed that for an observation interval of $[0,T_{\mathrm{o},i}]$, $x_i(t)$ is real and positive. The terms $\partial\tau_i/\partial P_{\mathrm{r},v_{(1|2)}}$, and $\partial\alpha_i/\partial P_{\mathrm{r},v_{(1|2)}}$ in (12) and (13) illustrate how the geometric configuration of the LED transmitters and photodetecting receiver (orientation, irradiance angle, incidence angle, and positioning) may have an impact. Even more, E^i_{A}, E^i_{AA}, E^i_{B}, E^i_{BB}, E^i_{C}, and E^i_{CC} in (14) denote the effect of the transmitted signals'

energies. Then, the effective CRLB of the positioning error can be obtained based on (9) from (10) as in [3]

$$\text{CRLB} \triangleq \text{trace}\left\{\mathcal{I}_{\text{sync}}^{-1}\right\}. \tag{15}$$

This expression provides the performance bounds for the 3D positioning accuracy evaluated in a synchronous VLP system under the effects of SDSN, which has not yet been studied in the literature.

Remark 1: The CRLB in (15) is the inverse of the FIM in (10). It can be observed that the ζ_n^2 term appears in the denominator and that as $\zeta_n^2 \to \infty$, in this case, the second summation $\sum_{i=1}^{L_{\text{T}}}\left(\frac{\partial\alpha_i}{\partial P_{\text{r},v_1}}\frac{\partial\alpha_i}{\partial P_{\text{r},v_2}}E_B^i + \alpha_i^2\frac{\partial\tau_i}{\partial P_{\text{r},v_1}}\frac{\partial\tau_i}{\partial P_{\text{r},v_2}}E_A^i - \alpha_i(\frac{\partial\alpha_i}{\partial P_{\text{r},v_1}}\frac{\partial\tau_i}{\partial P_{\text{r},v_2}} + \frac{\partial\tau_i}{\partial P_{\text{r},v_1}}\frac{\partial\alpha_i}{\partial P_{\text{r},v_2}})E_C^i\right) \to 0$. Consequently, $[\mathcal{I}_{\text{sync}}]$ becomes very small, which greatly increases the CRLB.

B. 3D Positioning Estimation in Quasi-Synchronous System

In this section, we study a quasi-synchronous VLP system operating under the effects of SDSN, where $\Delta_i = \Delta$ in (3) represents all the synchronized LED transmitters that have a timing bias with the photodetecting receiver. Here, the TDOA parameter is considered instead of TOA to eliminate the unknown deterministic parameter Δ from $\tau_i = \frac{\|\boldsymbol{P}_{\text{r}} - \boldsymbol{P}_{\text{t}}^i\|}{c} + \Delta$. The TDOA parameter measurements are computed by $(\tau_i - \tau_j)$, where τ_i and τ_j represent the TOA measurements at the photodetecting receiver from the ith and jth LED transmitters, and this happens for $i, j \in \{1, \ldots, L_{\text{T}}\}$ and $i \neq j$. Therefore, the scenario is termed hybrid TDOA-RSS. Now, based on (2), (3), and (4) the vector containing the set of unknown parameters in (7) becomes $\boldsymbol{\varrho} = [P_{r,x}\ P_{r,y}\ P_{r,z}\ \Delta]^T$. Now, from (7) and (8), the FIM $\mathcal{I}_{\text{qsyn}}$ can be derived by utilizing (11)–(13) and (14) as

$$[\mathcal{I}_{\text{qsyn}}] = \begin{bmatrix} \mathcal{I}_{\text{A}} & \mathcal{I}_{\text{b}} \\ \mathcal{I}_b^T & \mathcal{I}_{\text{d}} \end{bmatrix}, \tag{16}$$

$$\begin{aligned}
&[\mathcal{I}_{\text{A}}]_{v_1,v_2} \\
&= \frac{R^2}{\sigma_n^2}\Bigg(\zeta_n^4\,\sigma_n^2\sum_{i=1}^{L_{\text{T}}}\Bigg(\frac{\partial\alpha_i}{\partial P_{\text{r},v_1}}\frac{\partial\alpha_i}{\partial P_{\text{r},v_2}}E_{BB}^i + \alpha_i^2\frac{\partial\tau_i}{\partial P_{\text{r},v_1}}\frac{\partial\tau_i}{\partial P_{\text{r},v_2}}E_{AA}^i \\
&\quad - \alpha_i\left(\frac{\partial\alpha_i}{\partial P_{\text{r},v_1}}\frac{\partial\tau_i}{\partial P_{\text{r},v_2}} + \frac{\partial\tau_i}{\partial P_{\text{r},v_1}}\frac{\partial\alpha_i}{\partial P_{\text{r},v_2}}\right)E_{CC}^i\Bigg) \\
&\quad + \sum_{i=1}^{L_{\text{T}}}\Bigg(\frac{\partial\alpha_i}{\partial P_{\text{r},v_1}}\frac{\partial\alpha_i}{\partial P_{\text{r},v_2}}E_B^i + \alpha_i^2\frac{\partial\tau_i}{\partial P_{\text{r},v_1}}\frac{\partial\tau_i}{\partial P_{\text{r},v_2}}E_A^i \\
&\quad - \alpha_i\left(\frac{\partial\alpha_i}{\partial P_{\text{r},v_1}}\frac{\partial\tau_i}{\partial P_{\text{r},v_2}} + \frac{\partial\tau_i}{\partial P_{\text{r},v_1}}\frac{\partial\alpha_i}{\partial P_{\text{r},v_2}}\right)E_C^i\Bigg)\Bigg),
\end{aligned} \tag{17a}$$

$$\begin{aligned}
&[\mathcal{I}_{\text{b}}]_{v_{(1|2)},\Delta} \\
&= \frac{R^2}{\sigma_n^2}\left(\zeta_n^4\,\sigma_n^2\sum_{i=1}^{L_{\text{T}}}\left(\alpha_i^2\frac{\partial\tau_i}{\partial P_{\text{r},v_{(1|2)}}}E_{AA}^i - \alpha_i\frac{\partial\alpha_i}{\partial P_{\text{r},v_{(1|2)}}}E_{CC}^i\right)\right. \\
&\quad \left. + \sum_{i=1}^{L_{\text{T}}}\left(\alpha_i^2\frac{\partial\tau_i}{\partial P_{\text{r},v_{(1|2)}}}E_A^i - \alpha_i\frac{\partial\alpha_i}{\partial P_{\text{r},v_{(1|2)}}}E_C^i\right)\right),
\end{aligned} \tag{17b}$$

$$[\mathcal{I}_{\text{c}}]_{\Delta,\Delta} = \frac{R^2}{\sigma_n^2}\left(\zeta_n^4\,\sigma_n^2\sum_{i=1}^{L_{\text{T}}}\left(\alpha_i^2\,E_{AA}^i\right) + \sum_{i=1}^{L_{\text{T}}}\left(\alpha_i^2\,E_A^i\right)\right). \tag{17c}$$

Now, in the presence of the nuisance parameter Δ, the FIM $\mathcal{I}_{\text{qsyn}}$ can be calculated for the parameters of interest $\boldsymbol{P}_{\text{r}}$ from (16) based on (17) as in [22]

$$\mathcal{I}_{\text{qsyn}} = \left(\boldsymbol{\mathcal{I}}_A - \boldsymbol{\mathcal{I}}_b\boldsymbol{\mathcal{I}}_d^{-1}\boldsymbol{\mathcal{I}}_b^T\right). \tag{18}$$

Consequently, the effective CRLB is derived based on (9) from (18) after excluding the nuisance parameter Δ as

$$\text{CRLB} \triangleq \text{trace}\left\{\mathcal{I}_{\text{qsyn}}^{-1}\right\}. \tag{19}$$

Remark 2: It is key to note that the CRLB in (19) is larger than or equal to that in (15) due to estimation of the additional parameter. This can be explained by noting that $[\mathcal{I}_{\text{A}}] = [\mathcal{I}_{\text{sync}}]$. We can consequently affirm that

$$[\mathcal{I}_{\text{sync}}] - [\mathcal{I}_{\text{qsyn}}] \geq Z, \tag{20}$$

where $Z = \boldsymbol{\mathcal{I}}_b\boldsymbol{\mathcal{I}}_d^{-1}\boldsymbol{\mathcal{I}}_b^T$. Here Z is a positive semidefinite matrix because $\boldsymbol{\mathcal{I}}_b\boldsymbol{\mathcal{I}}_b^T$ and $\boldsymbol{\mathcal{I}}_d^{-1}$ are always positive. This means that the quasi-synchronous scenario is always worse than the synchronous one. It also means, though, that it approaches the performance of the synchronous scenario if $\Delta = 0$ or if the terms E_{A}^i, E_{AA}^i, E_{C}^i, and E_{CC}^i are zero.

C. 3D Positioning Estimation in Asynchronous System

This section studies the positioning error performance in an asynchronous VLC system under the effects of SDSN. In an asynchronous system, there exists a timing bias Δ_i between the photodetecting receiver and the LED transmitters clocks, where Δ_i is considered to be an unknown deterministic parameter for all $i \in \{1, \ldots, L_{\text{T}}\}$. Therefore, the relationship in (3) is unknown, meaning that the relationship between α_i and P_{r} from (2) needs to be exploited in order to estimate the position. This scenario is considered to be an RSS-based position estimation since α_i is related to RSS. Now, based on (2), (3), and (4) the vector containing the set of unknown parameters in (7) becomes $\boldsymbol{\varrho} = [P_{r,x}\ P_{r,y}\ P_{r,z}\ \tau]^T$, where $\tau = [\tau_1 \ldots \tau_{L_{\text{T}}}]$. Then, the FIM $\boldsymbol{\mathcal{I}}(\boldsymbol{\varrho_2})$ can be derived from (7) and (8) utilizing (11)–(13) and (14) as

$$[\mathcal{I}_{\text{asyn}}] = \begin{bmatrix} \mathcal{I}_{\text{A}} & \mathcal{I}_{\text{B}} \\ \mathcal{I}_B^T & \mathcal{I}_{\text{D}} \end{bmatrix}, \tag{21}$$

$$\begin{aligned}
[\mathcal{I}_{\text{A}}]_{v_1,v_2} &= \frac{R^2}{\sigma_n^2}\left(\zeta_n^4\,\sigma_n^2\sum_{i=1}^{L_{\text{T}}}\left(\frac{\partial\alpha_i}{\partial P_{\text{r},v_1}}\frac{\partial\alpha_i}{\partial P_{\text{r},v_2}}E_{BB}^i\right)\right. \\
&\quad \left. + \sum_{i=1}^{L_{\text{T}}}\left(\frac{\partial\alpha_i}{\partial P_{\text{r},v_1}}\frac{\partial\alpha_i}{\partial P_{\text{r},v_2}}E_B^i\right)\right),
\end{aligned} \tag{22a}$$

$$[\mathcal{I}_{\mathrm{B}}]_{v_{(1|2)},\tau_i} = -\frac{R^2}{\sigma_n^2}\,\alpha_i\,\frac{\partial \alpha_i}{\partial P_{\mathrm{r},v_{(1|2)}}}\left(\zeta_n^4\,\sigma_n^2\,E_{CC}^i + E_C^i\right), \tag{22b}$$

for $i, j \in \{1, \ldots, L_{\mathrm{T}}\}$ with

$$[\mathcal{I}_{\mathrm{D}}]_{\tau_i,\tau_j} = \begin{cases} \dfrac{R^2}{\sigma_n^2}\,\alpha_i^2\left(\zeta_n^4\,\sigma_n^2\,E_{AA}^i + E_A^i\right) & \text{if } i = j, \\ 0 & \text{otherwise.} \end{cases} \tag{22c}$$

Now, in the presence of the nuisance parameter τ_i for $i \in \{1, \ldots, L_{\mathrm{T}}\}$, the FIM $\mathcal{I}_{\mathrm{asyn}}$ for the parameters of interest $\boldsymbol{P}_{\mathrm{r}}$ can be calculated based on (21) from (22) as

$$\mathcal{I}_{\mathrm{asyn}} = \left(\boldsymbol{\mathcal{I}}_A - \boldsymbol{\mathcal{I}}_B\boldsymbol{\mathcal{I}}_D^{-1}\boldsymbol{\mathcal{I}}_B^T\right). \tag{23}$$

The effective CRLB can be subsequently derived from (9) and (23), after excluding the nuisance parameter τ_i, as

$$\mathrm{CRLB} \triangleq \mathrm{trace}\left\{\mathcal{I}_{\mathrm{asyn}}^{-1}\right\}. \tag{24}$$

Remark 3: Now, when $\zeta_n^2 = 0$ (i.e., suggesting no SDSN), all the terms in (15), (19), and (24) match perfectly with those in [6] and [13], hence validating the presented analysis.

IV. Simulation and Performance Analysis

In this section, the theoretical limits of the positioning estimation error performance are investigated with the help of simulation. We consider an area of $8 \times 8 \times 5\ m^3$ with a perpendicular distance of 4 m between the LED transmitters and the photodetecting receiver. There are $L_{\mathrm{T}} = 4$ LED transmitters placed at $P_{\mathrm{t}}^1 = [2\ 2\ 5]^T$, $P_{\mathrm{t}}^2 = [6\ 2\ 5]^T$, $P_{\mathrm{t}}^3 = [2\ 6\ 5^T]$, and $P_{\mathrm{t}}^4 = [6\ 6\ 5]^T$, respectively. The photodetecting receiver is placed at $P_{\mathrm{r}} = [4\ 4\ 1]^T$. The LED transmitters' orientation vectors are given as $\boldsymbol{n}_{\mathrm{t}}^i$, where $n_{\mathrm{t,x}}^i = \sin\theta_i \cos\phi_i$, $n_{\mathrm{t,y}}^i = \sin\theta_i \sin\phi_i$, and $n_{\mathrm{t,z}}^i = \cos\theta_i$, for $i \in \{1, 2, 3, 4\}$. The LED transmitters' orientation angles are set to $(\theta_1, \phi_1) = (150^\circ, 45^\circ)$, $(\theta_2, \phi_2) = (150^\circ, 135^\circ)$, $(\theta_3, \phi_3) = (150^\circ, -45^\circ)$, and $(\theta_4, \phi_4) = (150^\circ, -135^\circ)$. The photodetecting receiver's orientation $\boldsymbol{n}_{\mathrm{r}}$ is chosen as $\boldsymbol{n}_{\mathrm{r}} = [0\ 0\ 1]^T$. The LED transmitters' Lambertian order is $m_i = 1$, and the VLC photodetector's responsivity is assumed to be $R = 1$ A/W with an area A_{P} of 3×3 cm^2. The noise variance is $\sigma_n^2 = 10^{-10}$ W, $\zeta_n^2 \in [0, 10]$, and the signal $x_i(t)$ in (4) is modeled as

$$x_i(t) = A\left(1 - \cos\left(2\,\pi\,t/T_{\mathrm{o},i}\right)\right)\left(1 + \cos\left(2\,\pi\,f_c\,t\right)\right), \tag{25}$$

where $A = 30$ dBm is the source optical power applied with a signal duration of $T_{\mathrm{o},i} = 10^{-5}$ s and a carrier frequency of $f_c = 100$ MHz. The aforementioned parameters in Table I remain constant unless otherwise stated.

Fig. 2 studies the effect of ζ_n^2 on the CRLBs for synchronous, quasi-synchronous, and asynchronous scenarios. The CRLB for each scenario has the lowest value when $\zeta_n^2 = 0$ (i.e., no SDSN). However, as ζ_n^2 increases, SDSN impacts the estimation bounds in all the cases, which is evident from the figure. For instance, error bounds at $\zeta^2 = 0$ and $\zeta^2 = 10$ for the synchronous scenario is about 8.7 cm and 10.2 cm, whereas for the quasi-synchronous scenario it is about 28.2 cm and 35 cm, and for the asynchronous scenario it is about 55.3 cm and 70 cm.

TABLE I
Parameters Data Sheet

Parameter	Value
Room dimension (L x W x H)	8 x 8 x 5 m^3
LEDs height (h)	4 m
Number of LEDs (L_{T})	4
Positions of LEDs	$P_{\mathrm{t}}^1 = [2\ 2\ 5]^T$ $P_{\mathrm{t}}^2 = [6\ 2\ 5]^T$ $P_{\mathrm{t}}^3 = [2\ 6\ 5]^T$ $P_{\mathrm{t}}^4 = [6\ 6\ 5]^T$
Orientations of LEDs	$n_{\mathrm{t}}^i = [\sin\theta_i \cos\phi_i \ \ \sin\theta_i \sin\phi_i \ \ \cos\theta_i]^T$ $(\theta_1, \phi_1) = (150^\circ, 45^\circ)$ $(\theta_2, \phi_2) = (150^\circ, 135^\circ)$ $(\theta_3, \phi_3) = (150^\circ, -45^\circ)$ $(\theta_4, \phi_4) = (150^\circ, -135^\circ)$
Position of photodetector	$P_{\mathrm{r}} = [4\ 4\ 1]^T$
Orientation of photodetector	$n_{\mathrm{r}} = [0\ 0\ 1]^T$
Photodetector's responsitivity	1 A/W
Photodetector's area	3 x 3 cm^2
Noise variance	$\sigma_n^2 = 10^{-10}$ W
SDSN scaling factor	$\zeta_n^2 \in [0, 10]$

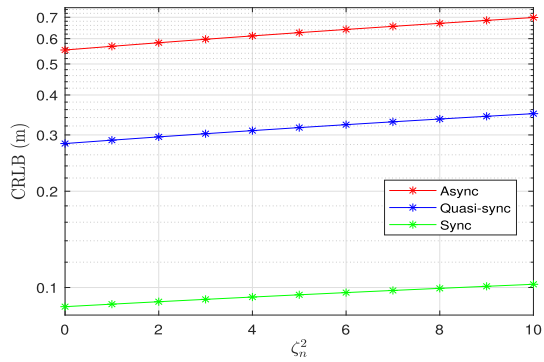

Fig. 2. CRLB versus ζ_n^2 for synchronous, quasi-synchronous, and asynchronous scenarios.

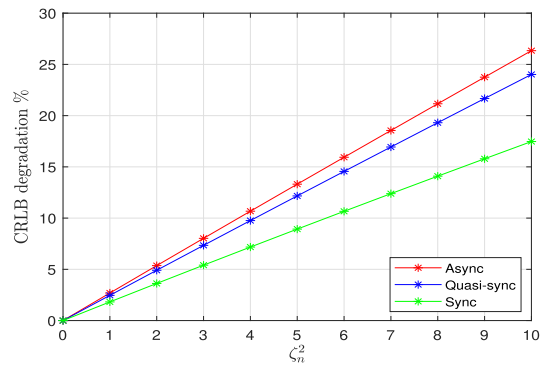

Fig. 3. CRLB degradation % versus ζ_n^2 for synchronous, quasi-synchronous, and asynchronous scenarios.

Fig. 3 illustrates the error bound degradation in the presence of SDSN for all considered scenarios. We calculate the CRLB degradation as

$$CRLB_{deg} = \left(\frac{CRLB_{\zeta_n^2>0}}{CRLB_{\zeta_n^2=0}} - 1\right) \times 100\%. \tag{26}$$

The CRLBs are obtained using (15), (19), and (24) for synchronous, quasi-synchronous, and asynchronous scenarios,

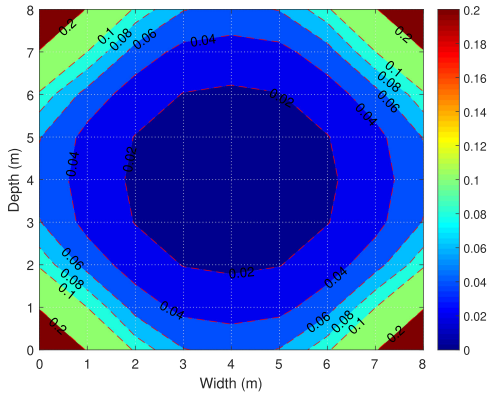

(a) CRLB with $\zeta_n^2 = 0$.

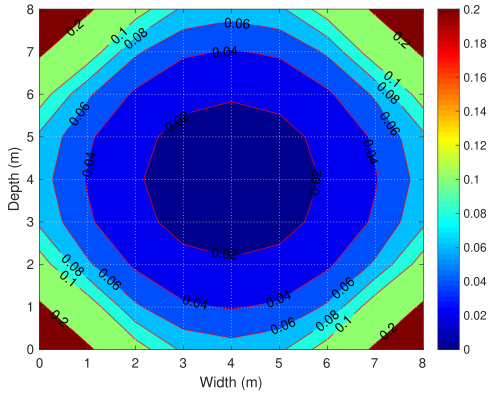

(b) CRLB with $\zeta_n^2 = 20$.

Fig. 4. CRLB as the photodetector receiver moves inside the space for synchronous scenario, where $T_{o,i} = 10^{-4}$s.

respectively. The asynchronous scenario shows the worst performance with a degradation level of 26.3% when $\zeta_n^2 = 10$, followed by the quasi-synchronous scenario with a degradation level of 24.01% and the synchronous scenario with a degradation level of 17.47%. This behaviour can be explained by noting that the asynchronous position estimation relies only on the α_i parameter, which is related to RSS. So as RSS increases, the SDSN has more of an impact on the error bounds for the asynchronous scenario compared to the synchronous and quasi-synchronous scenarios, which makes sense since these scenarios use both α_i and τ_i parameters.

Fig. 4 shows the contour plots used to study the effect of ζ_n^2 on the error bounds for the synchronous scenario. The photodetecting receiver moves inside the considered area along the edge from the $\boldsymbol{P}_{\mathrm{r}} = [0\ 0\ 1]^T$ to the $\boldsymbol{P}_{\mathrm{r}} = [8\ 8\ 1]^T$ positions.

Fig. 4(a) illustrates the CRLB when $\zeta_n^2 = 0$ (i.e., no SDSN) and Fig. 4(b) shows the CRLB when $\zeta_n^2 = 20$. The result here agrees with the ones in the previous figure, where ζ_n^2 has a negative impact on the error bounds because the contour area for each one is smaller when SDSN is present. In addition, as the figure shows, when the photodetecting receiver is placed at the edges, SDSN has less of an impact on the error bounds. This is due to the fact that the signal strength decreases when moving away from the LED transmitters. This confirms that the impact of SDSN depends on the RSS. The quasi-synchronous and asynchronous scenarios demonstrated a similar trend, so their figures were not included.

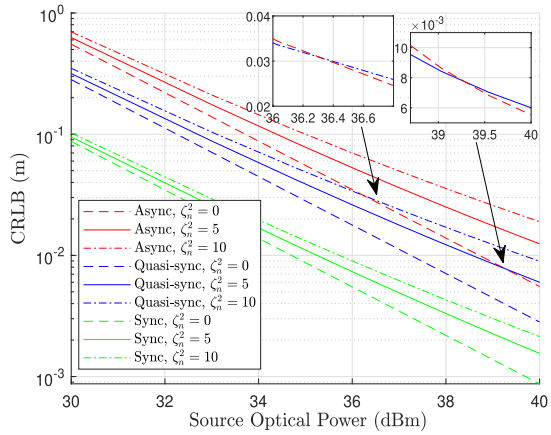

Fig. 5. CRLB versus source optical power for synchronous, quasi-synchronous, and asynchronous scenarios.

Finally, in Fig. 5, the CRLBs for synchronous, quasi-synchronous, and asynchronous scenarios are plotted against the source optical power A for different values of ζ_n^2. As anticipated, a higher source optical power improves the CRLBs for all considered scenarios. Moreover, the synchronous scenario still demonstrates the best performance for all the studied energy and ζ_n^2 values. However, as can be seen, the presence of SDSN mitigates the effect of increasing optical power at the source. For example, in the quasi-synchronous scenario, a 1.0 dBm power loss between $\zeta_n^2 = 0$ and $\zeta_n^2 = 10$ is observed when the CRLB $= 10^{-1}$. This loss increases to more than 2.0 dBm when the CRLB $= 10^{-2}$. The same trend is observed in both the synchronous and asynchronous scenarios.

Moreover, there is a point where the performance of the quasi-synchronous scenario at $\zeta_n^2 = 10$ is eclipsed by that of the asynchronous scenario at $\zeta_n^2 = 0$. This can be observed in the subplot where the blue and red lines intersect (i.e., the quasi-synchronous scenario demonstrates better performance before a source optical power of 36.4 dBm, and poor performance afterwards). The same behaviour can be observed between the quasi-synchronous at $\zeta_n^2 = 5$ and the asynchronous scenario at $\zeta_n^2 = 0$. In this case, the point of intersection shifts to the right towards 39.2 dBm.

V. Conclusion

This paper presents the theoretical CRLBs for a 3D VLP system under the effects of SDSN. We consider three different scenarios, and it was shown that the SDSN has a severe impact on the estimation bounds in all studied scenarios. Furthermore, it was observed that the degradation level is higher for the asynchronous scenario when the position estimation is based only on the channel attenuation factor, which is related to RSS, and is impacted more by the presence of SDSN. In comparison, when the position estimation considers both the channel attenuation factor and either the time of arrival or the time difference of arrival parameters, the VLP systems are impacted much less. In future works, estimators that can correspond to the CRLB's

performance in a system under the effects of SDSN will be considered.

REFERENCES

[1] Y. Zhuang *et al.*, "A survey of positioning systems using visible LED lights," *IEEE Commun. Surv. Tut.*, vol. 20, no. 3, pp. 1963–1988, Jul.–Sep. 2018.

[2] M. Afzalan and F. Jazizadeh, "Indoor positioning based on visible light communication: A performance-based survey of real-world prototypes," *ACM Comput. Surv.*, vol. 52, no. 2, pp. 1–36, 2019.

[3] S. M. Kay, *Fundamentals of Statistical Signal Processing*. Englewood Cliffs, NJ, USA: Prentice-Hall, 1993.

[4] T. Q. Wang, Y. A. Sekercioglu, A. Neild, and J. Armstrong, "Position accuracy of time-of-arrival based ranging using visible light with application in indoor localization systems," *J. Lightw. Technol.*, vol. 31, no. 20, pp. 3302–3308, 2013.

[5] C. Amini, A. Taherpour, T. Khattab, and S. Gazor, "Theoretical accuracy analysis of indoor visible light communication positioning system based on time-of-arrival," in *Proc. IEEE Can. Conf. Elect. Comput. Eng.*, 2016, pp. 1–5.

[6] M. F. Keskin, A. D. Sezer, and S. Gezici, "Localization via visible light systems," *Proc. IEEE*, vol. 106, no. 6, pp. 1063–1088, Jun. 2018.

[7] A. Naeem, N. U. Hassan, M. A. Pasha, C. Yuen, and A. Sikora, "Performance analysis of TDOA-based indoor positioning systems using visible LED lights," in *Proc. IEEE 4th Int. Symp. Wireless Syst. Within Int. Conf. Intell. Data Acquisition Adv. Comput. Syst.*, 2018, pp. 103–107.

[8] X. Zhang, J. Duan, Y. Fu, and A. Shi, "Theoretical accuracy analysis of indoor visible light communication positioning system based on received signal strength indicator," *J. Lightw. Technol.*, vol. 32, no. 21, pp. 3578–3584, 2014.

[9] Z. Zheng, L. Liu, and W. Hu, "Accuracy of ranging based on DMT visible light communication for indoor positioning," *IEEE Photon. Technol. Lett.*, vol. 29, no. 8, pp. 679–682, Apr. 2017.

[10] H. Hosseinianfar and M. Brandt-Pearce, "Performance limits for fingerprinting-based indoor optical communication positioning systems exploiting multipath reflections," *IEEE Photon. J.*, vol. 12, no. 4, Aug. 2020, Art. no. 7903416.

[11] X. Liu, D. Zou, N. Huang, and S. Zhang, "A comprehensive accuracy analysis of visible light positioning under shot noise," in *Proc. IEEE/CIC Int. Conf. Commun. China Workshops*, 2020, pp. 167–172.

[12] B. Zhou, Y. Zhuang, and Y. Cao, "On the performance gain of harnessing non-line-of-sight propagation for visible light-based positioning," *IEEE Trans. Wireless Commun.*, vol. 19, no. 7, pp. 4863–4878, Jul. 2020.

[13] E. Kazikli and S. Gezici, "Hybrid TDOA/RSS based localization for visible light systems," *Digit. Signal Process.*, vol. 86, pp. 19–28, 2019.

[14] H. Steendam, T. Q. Wang, and J. Armstrong, "Theoretical lower bound for indoor visible light positioning using received signal strength measurements and an aperture-based receiver," *J. Lightw. Technol.*, vol. 35, no. 2, pp. 309–319, 2016.

[15] L. E. M. Matheus, A. B. Vieira, L. F. Vieira, M. A. Vieira, and O. Gnawali, "Visible light communication: Concepts, applications and challenges," *IEEE Commun. Surv. Tut.*, vol. 21, no. 4, pp. 3204–3237, Oct.–Dec. 2019.

[16] S. M. Moser, "Capacity results of an optical intensity channel with input-dependent Gaussian noise," *IEEE Trans. Inf. Theory*, vol. 58, no. 1, pp. 207–223, Jan. 2012.

[17] Q. Gao, K. Qaraqe, and E. Serpedin, "Improving the modulation designs for visible light communications with signal-dependent noise," *IEEE Commun. Mag.*, vol. 58, no. 5, pp. 26–32, May 2020.

[18] J.-Y. Wang, J.-B. Wang, and Y. Wang, "Fundamental analysis for visible light communication with input-dependent noise," *Opt. Fiber Wireless Commun.*, 2017, pp. 143–157.

[19] J.-Y. Wang, X.-T. Fu, R.-R. Lu, J.-B. Wang, M. Lin, and J. Cheng, "Tight capacity bounds for indoor visible light communications with signal-dependent noise," *IEEE Trans. Wireless Commun.*, vol. 20, no. 3, pp. 1700–1713, Mar. 2021.

[20] M. Yaseen, M. Alsmadi, A. E. Canbilen, and S. S. Ikki, "Visible light communication with input-dependent noise: Channel estimation, optimal receiver design and performance analysis," *J. Lightw. Technol.*, vol. 39, no. 23, pp. 7406–7416, 2021.

[21] J. M. Kahn and J. R. Barry, "Wireless infrared communications," *Proc. IEEE*, vol. 85, no. 2, pp. 265–298, Feb. 1997.

[22] Y. Zhu and N. Reid, "Information, ancillarity, and sufficiency in the presence of nuisance parameters," *Can. J. Statist.*, vol. 22, no. 1, pp. 111–123, 1994.